ELSEVIER

Earth and Planetary Science Letters 140 (1996) 27–39

EPSL

The influence of trench migration on slab penetration into the lower mantle

Ulrich R. Christensen *

Institut für Geophysik, Universität Göttingen, Herzberger Landstrasse 180, 37075 Göttingen, Germany

Received 26 October 1995; accepted 9 February 1996

Abstract

A two-dimensional numerical convection model in cartesian geometry is used to study the influence of trench migration on the ability of subducted slabs to penetrate an endothermic phase boundary at 660 km depth. The transient subduction history of an oceanic plate is modelled by imposing plate and trench motion at the surface. The viscosity depends on temperature and depth. A variety of styles of slab behaviour is found, depending predominantly on the trench velocity. When trench retreat is faster than 2–4 cm/a, the descending slab flattens above the phase boundary. At slower rates it penetrates straight into the lower mantle, although flattening in the transition zone may occur later, leading to a complex slab morphology. The slab can buckle, independent of whether it penetrates or not, especially when there is a localised increase in viscosity at the phase boundary. Flattened slabs are only temporarily arrested in the transition zone and sink ultimately into the lower mantle. The results offer a framework for understanding the variety in slab geometry revealed by seismic tomography.

Keywords: lower mantle; slabs; trenches; subduction

1. Introduction

A key question in geodynamics is whether lithospheric slabs penetrate into the lower mantle or if they remain in the upper mantle. Recent results from the tomographic mapping of subduction zones and from numerical convection modelling suggest that the behaviour of slabs at the 660 km seismic discontinuity could be more complex and variable than was previously thought. For the Western Pacific subduction zones, there is evidence for slab penetration into the lower mantle beneath the Northern Kurile, Mariana and Tonga arcs, whereas flat-lying slabs above the 660 km discontinuity are found beneath the Southern Kuriles, Japan, Java and the Izu–Bonin trenches [1,2]. Beneath the Americas, Grand [3] has mapped slab-like structures in the lower mantle in regions of past subduction but, due to a lack of resolution, their geometry in the transition zone could not be reliably determined. Beneath Northern Tonga a complex morphology is found, with the slab lying subhorizontally above the 660 km discontinuity for about 800 km length, before it seems to descend into the lower mantle at greater distance from the Tonga trench [4]. In the cases of the Tonga and Izu–Bonin slabs, Van der Hilst and co-workers [4,5] have proposed that the failure for penetration is caused by

* Tel.: +49 551 39 7451; Fax: +49 551 39 7459; E-mail: urc@willi.uni-geophys.gwdg.de

PII S0012-821X(96)00023-4

fast trench rollback (migration in the direction of the subducting plate), which should induce the slab to lie down on the 660 km discontinuity. In comparison, adjacent slabs that seem to penetrate directly into the lower mantle exhibit less rollback. Global [6] and regional [7] studies of the topography of the 660 km discontinuity show that subduction zones are associated with depressions of the discontinuity, especially in regions with flat-lying slabs.

There is little doubt now that the 660 km discontinuity is caused by the endothermic transformation of γ-spinel into perovskite and magnesiowüstite [8]. A slight change in composition might be superimposed, but it would contribute less than 2% of intrinsic density contrast [9], which alone is insufficient to arrest a sinking slab [10]. The Clapeyron slope for the transformation of γ-spinel is approximately -2 to -3 MPa/K [8,11]. While earlier modelling [10,12] demonstrated that an endothermic phase change could, in principle, arrest slabs and cause two-layer mantle convection, it also suggested that this would require a more negative value of the Clapeyron slope. Recently, a number of authors, using realistic model geometry and revised estimates for the thermal expansion coefficient in the deep mantle, demonstrated that, with plausible values of the Clapeyron slope, a hybrid mode of mantle convection is possible (e.g., [13–15]). Typically, in these simulations, the circulation is found to be at least regionally layered for extended periods of time, during which cold downwelling fluid accumulates above the phase boundary. Then, in a so-called avalanche event, the ponded material sinks rapidly into the lower mantle. In the Earth's mantle, subduction of slabs is certainly the most significant mode of downwelling. Downwellings in the basically isoviscous models exhibiting the avalanche behaviour do not represent three important characteristics of subduction: (1) because of their low temperature, slabs are rheologically distinct from the ambient mantle; (2) subduction is non-symmetric and consequently slabs usually descend at an oblique angle, whereas the downwellings in simple convection models sink vertically; (3) convergence zones at the Earth's surface migrate, whereas the location of major downwellings in most previous models remains stationary.

Christensen and Yuen [10] used a temperature and stress-dependent rheology to model the interaction of slabs with a phase boundary. Zhong and Gurnis [16] modelled plate-like behaviour with temperature-dependent viscosity and by the introduction of weak zones into the high-viscosity lid. They found that plates penetrate more easily through an endothermic phase boundary than isoviscous convection currents and that the penetration occurs in a more steady fashion. However, in both cases [10,16] subduction was forced to occur vertically along the side boundaries of the model domain. Using a model with temperature-dependent viscosity, where plate-like motion was imposed by a velocity boundary condition at the surface and subduction occurred at a fixed place in the centre of the model box, Davies [17] showed that high-viscosity slabs are more likely to penetrate than low-viscosity plumes, and that the Clapeyron slope must be more negative than -3 MPa/K in order to avoid immediate penetration. King and Ita [18] obtained a similar result in a model without surface forcing. The highest degree of realism so far has been achieved in a model of Zhong and Gurnis [19], where one-sided subduction and trench migration were facilitated by means of a movable 'fault zone' within the high-viscosity lid at the surface. In this model the subducted slab flattens initially above the phase boundary while the trench moves in a retrograde direction. Later, the slab breaks through the phase boundary and trench migration ceases.

The role of trench migration has also been studied in laboratory experiments [20–22], where highly viscous 'slabs' of corn syrup sink and impinge upon an interface between two layers differing in density and viscosity. A wide range of possible slab behaviour was found, mainly controlled by the rate of trench migration in relation to the free sinking velocity of the slab. Fast trench movement generally prevents penetration into the lower layer. A difference between these model systems and the Earth's mantle is that the main resistance against penetration through the 660 km discontinuity is thought to be the strong and localised buoyancy force due to the downward deflection of the phase boundary, whereas in the laboratory models it is the higher viscosity and/or density of the lower layer.

Here I extend the model calculations of Davies [17] by adding trench migration, which is demonstrated to have a major influence. Depending on its

rate and other control parameters, slabs behave quite differently when they impinge upon an endothermic phase boundary.

2. Model set-up

Thermal convection in a two-dimensional cartesian model box 8000 km long and 2500 km deep is studied using the Boussinesq approximation (Fig. 1a). At the surface, the horizontal velocity, u, is controlled by a boundary condition $u = U(x,t)$. $U(x,t)$ describes the motion of a plate with a constant velocity U_{Plate}. The spreading ridge is at the left edge of the box ($x = 0$). In most cases $U_{Plate} = 5$ cm/a. In the subduction zone, the velocity changes over a 225 km wide transition region to a negative value $-U_{Trench}$ (Fig. 1b); an overshoot in the velocity profile helps to prevent the attachment of the sinking plate to the surface on the right of the subduction point. However, in some cases the slab gets attached to the surface at a later stage and the calculation is then stopped. The subduction zone is initially at $x = 5000$ km and moves at a constant rate, U_{Trench}, towards the ridge. The calculation is stopped when the trench has migrated to $x = 2000$ km. The surface temperature is set to 0°C for the region of the subducting plate, but towards the right of the subduction zone it equals the temperature in the interior of the mantle (Fig. 1c), which is set to $T_o = 1300$°C as initial condition. For the subducting plate, an error function geotherm is assumed with a linear increase of its nominal age up to a value of $t_o = 100$ Ma at the subduction zone. The overriding plate is not modelled in order to keep the set-up as simple as possible. At the side boundaries mirror symmetry is assumed. The bottom boundary is semi-permeable in most cases. Here, the shear stress is zero and the vertical normal stress, σ_{zz}, is proportional to the vertical velocity, w (Fig. 1a), such that there is some resistance against flow out of or into the box. The constant of proportionality, R, was chosen such that the resistance is similar to that offered by a half-space with the same viscosity as at the bottom of the model. The reason for employing this peculiar condition will be discussed later. The Biot-type thermal condition at the bottom (Fig. 1a) is essentially one of zero heat flux, in order to avoid additional complications of rising plumes in the model, but it also ensures that any inflowing material has the background temperature, T_o. There is no internal heating. The viscosity, η, is a function of temperature, T, and depth, z:

$$\eta = \eta_o \exp\left(T_o - T\right)/a + z/b - (z/c)^2 \qquad (1)$$

The parameters ($\eta_o = 10^{20}$ Pa s, $a = 131.3$ K, $b = 236$ km, $c = 1086$ km) imply a change of viscosity with temperature between 0°C and 1300°C by a factor of 2×10^4, and a variation with depth by a factor of 200 (Fig. 2). The average viscosities of the upper and lower mantle differ by a factor of approxi-

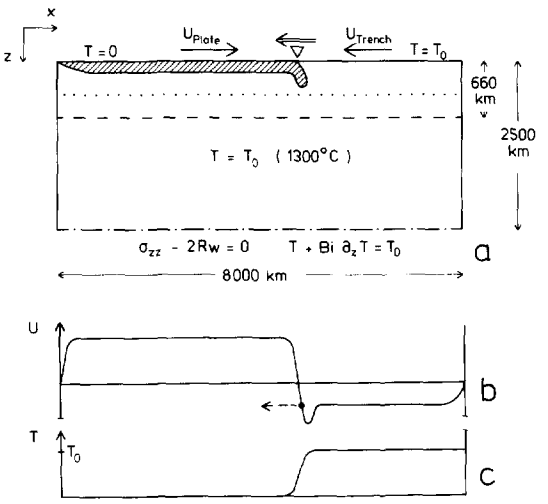

Fig. 1. (a) Model concept. Bi is a Biot parameter and R controls the resistance against flow through the open bottom boundary. (b) Imposed surface velocity as a function of x (schematic). (c) Imposed temperature at the surface.

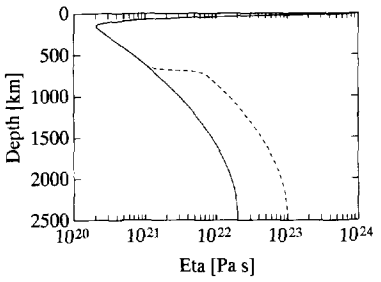

Fig. 2. Viscosity as a function of depth at $t = 0$ and $x = 4000$ km. The full line is the standard case, the broken line a case with an additional five-fold increase at the phase boundary.

mately 10–30, which agrees with estimates from geoid analyses [23,24], but viscosity is assumed to vary smoothly rather than discontinuously at the phase boundary. In a few model runs, the influence of an additional jump in viscosity at 660 km is also studied. The variation of viscosity with temperature is weaker than in experimentally determined flow laws, but the additional stress-dependence of the rheology, which is not explicitly accounted for in the model, would tend to reduce the influence of temperature on the strength of slabs [25]. The thermal expansion coefficient, α, decreases exponentially with depth by a factor of six [26], and the other material properties are constant (Table 1). The thermal Rayleigh number, evaluated with the properties at z = 410 km and 1300°C and based on the temperature difference between surface and interior, is 4.2×10^7.

For the endothermic phase change boundary near 660 km depth, a Clapeyron slope of -2.8 MPa/K and a density contrast of 9% are assumed in most cases [8]. The phase boundary is modelled by a chain of tracers whose depth is controlled by temperature [10]. Buoyancy forces arise from deflections of the phase boundary. The effects of latent heat, which are thought to be of minor influence [12,27], are ignored within the Boussinesq approximation.

The equations of viscous flow are formulated as a generalised biharmonic equation for the stream-function and are solved by a finite element method based on bicubic splines. Temperature is represented by biquadratic splines and is advanced by a predictor-corrector method. Technical details can be found elsewhere [10,25,28]. The mesh consists of 240×40 non-uniform elements with fine spacing in the upper mantle and the transition zone and coarse spacing below 1000 km depth.

In order to verify that the imposed surface velocity agrees on an order-of-magnitude scale with the velocity of free convection for the chosen parameters, the sinking velocity of a vertically dipping 'detached slab' with a thermal anomaly equivalent to that of 100 Ma old lithosphere was determined for a free-slip surface kept at temperature T_0 everywhere (no surface plate). Velocities in the range of 5–12 cm/a are obtained, depending on whether the slab extends to 600 or to 1200 km depth (down from 200 km) and whether the endothermic phase boundary is included.

Table 1
Notation and standard model parameters

	Symbol	Value
Density	ρ	4000 kg m^{-3}
Gravity	g	10 m s^{-2}
Thermal expansion coeff.	α	variable
- surface value	α_0	3.5×10^{-5} K^{-1}
Temperature contrast	T_0	1300 K
Height	h	2.5×10^6 m
Thermal diffusivity	κ	10^{-6} $m^2 s^{-1}$
Viscosity	η	variable
Heat capacity	c_p	1250 J kg^{-1} K^{-1}
Plate velocity	U_{Plate}	5 cm/a
Trench velocity	U_{Trench}	variable
Initial plate age at trench	t_0	100 Ma
Density contrast at 660 km	$\Delta\rho$	360 kg m^{-3}
Clapeyron slope	γ	-2.8 MPa K^{-1}
Biot parameter	Bi	1.25×10^6 m
Bottom resistance	R	1.26×10^{13} Pa s m^{-1}

3. Results

3.1. Standard model parameters

In the first series of experiments, the influence of the rate of trench migration on slab behaviour was studied for the standard set of model parameters, as described in the previous section and in Table 1. When the trench is stationary, the slab descends vertically and immediately penetrates into the lower mantle, even when the Clapeyron slope γ is reduced to -4 MPa/K (cases STD0 and CL40-0; see Table 2 for a summary of all model runs). This agrees with Davies' [17] result for free-slip side boundaries. With periodic boundaries, Davies observed that the slab bends around at $\gamma = -4$ MPa/K and moves horizontally above the phase boundary. However, in his model the entire lower mantle is moving along, with the flat-lying slab almost as a rigid block, so that there is no shear stress acting on the slab from below. In my model the sinking slab is stopped when γ is reduced to the probably unrealistic values of -4.8 or -5.6 MPa/K (CL48-0 and CL56-0). It then folds and forms a large, cold block resembling the 'megalith' envisioned by Ringwood and Irifune [29]. Later, it sinks into the lower mantle (Fig. 3).

In models that include trench rollback, but ignore the dynamic effects of the phase boundary (NPH1, NPH3), slabs with nearly constant dip angles of 60° and 40° down to the bottom of the model box are obtained after 80 Ma for $U_{Trench} = 1$ cm/a and 3 cm/a, respectively (Fig. 4a). When the influence of the phase boundary is included, no penetration is observed for the duration of the model run (80 Ma) for trench velocities of 3 cm/a or higher (cases STD3–STD5, Fig. 4b). The slab flattens above the phase boundary (labelled style F in Table 2) and thickens mainly by thermal diffusion. Advective thickening was monitored using tracer particles and amounts to less than 20% until the end of the run. With $U_{Trench} = 2$ cm/a (STD2), penetration is somewhat retarded (style RP), but after a few million years the slab breaks through, dragging the initially flat-lying short slab segment down (Fig. 4c). This gives rise to a peculiar hook-structure of the slab in the lower mantle. Eventually straight penetration ceases and a flat slab segment forms again (Fig. 4d). At this stage, the pattern of the thermal anomaly resembles that of the seismic anomalies in Northern Tonga [4] (style FE).

In order to monitor slab flux, the amount of advected heat at 300 km and 750 km depth has been recorded and is displayed for various cases in Fig. 5. Because the initial stratification of the mantle is adiabatic in the model, there is no resistance against mass transfer through the phase boundary outside

Table 2
Summary of models

Model	U_{Trench} [cm/a]	Non-standard property	Pn [%]	Style
NPH1	1	Δρ=0	97	P
NPH3	3	Δρ=0	94	P
STD0	0		98	P
STD1	1		77	P-FE
STD2	2		70	RP-FE
STD3	3		5	F
STD4	4		3	F
STD5	5		2	F
STD1-3	1-3	Utrench changes	68	P-FE
STD3-1	3-1	Utrench changes	85	FS-FE
BCLS1	1	Bottom closed	90	P-FE-FS
BCLS2	2	Bottom closed	61	RP-FE
BNOR1	1	No bottom resistance	99	P
BNOR2	2	No bottom resistance	98	RP-P
BNOR3	3	No bottom resistance	7	F
HVIS1	1	Higher viscosity	75	RP-FE
HVIS2	2	Higher viscosity	11	F
LVIS2	2	Lower viscosity	78	RP-FE
LVIS3	3	Lower viscosity	7	F
UPL82	2	Uplate = 8 cm/a	66	RP-FE
UPL83	3	Uplate = 8 cm/a	14	F (B)
UPL84	4	Uplate = 8 cm/a	5	F
UPL31	1	Uplate = 3 cm/a	83	RP-FE
UPL32	2	Uplate = 3 cm/a	10	F
UPL113	3	Uplate = 11 cm/a	77	RP-FE
LDC3	3	Δρ/ρ = 6%	76	RP-FE
LDC4	4	Δρ/ρ = 6%	10	F
OLS3	3	Oliv.-spinel trans. add.	72	FS-FE
OLS4	4	Oliv.-spinel trans. add.	4	F
VSTP1	1	Viscosity step added	77	P-FE(B)
VSTP2	2	Viscosity step added	10	F (B)
VSTP3	3	Viscosity step added	8	F
NPHV1	1	Viscosity step, Δρ = 0	93	P (B)
NPHV2	2	Viscosity step, Δρ = 0	87	P
AGE50.2	2	Initial age 50 Ma	80	RP
AGE50.3	3	Initial age 50 Ma	1	F
AGE150.3	3	Initial age 150 Ma	9	F
AVIS0	0	Slab has ambient visc.	68	FD
AVIS1	1	Slab has ambient visc.	75	FD
AVIS2	2	Slab has ambient visc.	59	FD
AVIS3	3	Slab has ambient visc.	11	F
CL40-0	0	Clapeyron slope -4.0	94	P
CL48-0	0	Clapeyron slope -4.8	95	PIL-SP
CL56-0	0	Clapeyron slope -5.6		PIL-SP

Pn: Amount of slab in the lower mantle relative to total subducted slab. Styles: **P** = straight penetration of slab; **RP** = retarded penetration; **F** = flat slab without penetration; **FE** = flat slab, penetrating at its end; **FD** = flat slab, penetrating by diapiric instability; **FS** = flat slab, penetration triggered near subduction zone and flat segment dragged into lower mantle; **PIL** = slab folding and piling up; **SP** = pile sinking into lower mantle; **(B)** = buckling.

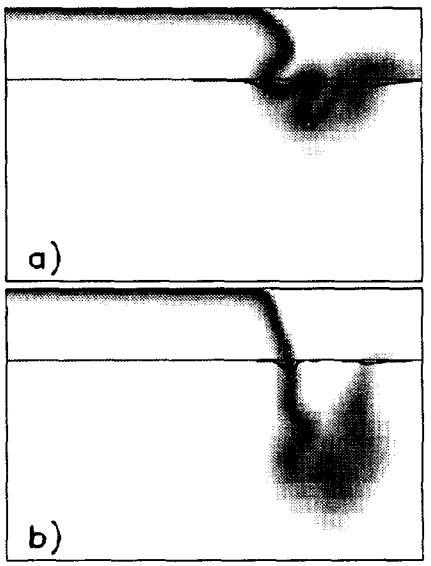

Fig. 3. Model CL56-0 with no trench motion and a Clapeyron slope of −5.6 MPa/K. Temperature in grey scale, plus the actual and the reference position of the phase boundary are shown. Only the part of the model between x = 2660 km and 6460 km is displayed. (a) After 119 Ma. (b) After 149 Ma.

regions of anomalous temperature (slabs); therefore monitoring the mass flux would be meaningless in this kind of model. Even in cases where the slab proper does not penetrate, a weak advective flux is observed at 750 km (e.g. Fig. 5c). This is due to the thermal halo of the slab, which penetrates below the phase boundary and is entrained in lower mantle flow. In cases where, after initial penetration, the slab flattens later (FE, example in Fig. 4d), the flux into the lower mantle remains significant, approximately 40% of the subduction flux in the case STD2 (Fig. 5b). Therefore, the flat slab segment continually bends around at its end and descends into the lower mantle. The accumulated amount of cold material (Pn) that has descended into the lower mantle at the end of a model run, relative to what could have potentially descended assuming vertical dip and uninhibited flux, is less than 10% in cases of flattened slabs (F) and typically more than 70% for partial penetration (Table 2).

For 1 cm/a trench rollback, the descending slab penetrates without delay into the lower mantle (style P), similar to Fig. 4a. However, the subsequent evolution depends on the nature of the bottom boundary condition. With the standard condition (STD1), straight penetration lasts for approximately 100 Ma; subsequently a flat-lying slab segment develops (style FE), similar to case STD2. In this stage the slab flux into the lower mantle is about 60% of the subduction flux (Fig. 5a). When the parameter R in the bottom boundary condition is set to zero; that is, there is no resistance against flow through the

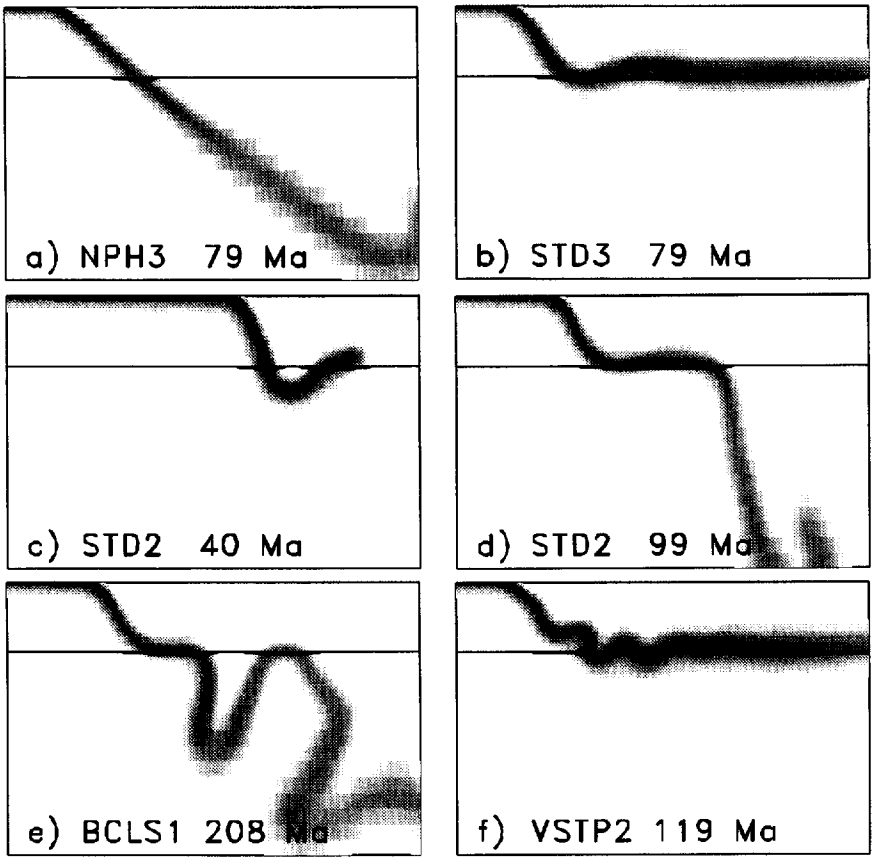

Fig. 4. Models with trench migration and standard physical parameters. The region between the actual depth of the phase boundary and its reference depth shown in dark. Only the part between x = 2080 km and 5880 km is shown. (a) No density contrast associated with the phase boundary, U_{Trench} = 3 cm/a. (b) Standard phase boundary, U_{Trench} = 3 cm/a. (c) U_{Trench} = 2 cm/a. (d) Same at later time. (e) Bottom boundary closed, U_{Trench} = 1 cm/a. (f) Additional stepwise viscosity increase at the phase boundary, U_{Trench} = 2 cm/a.

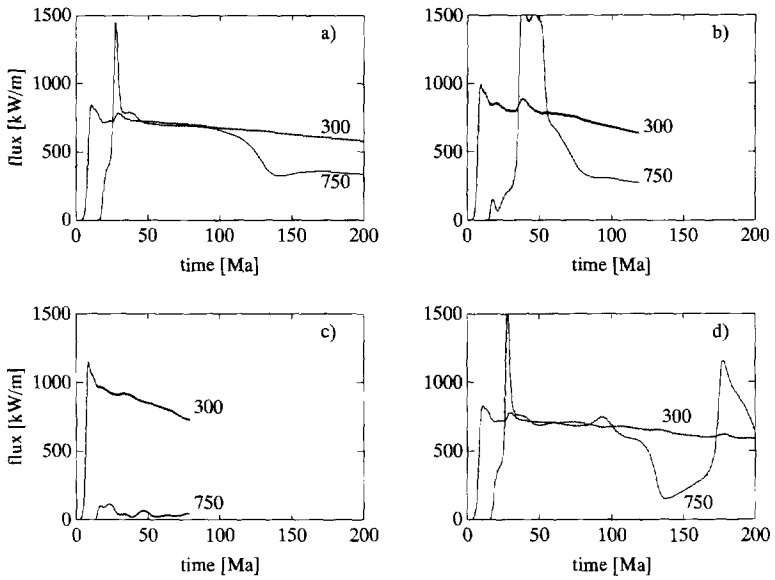

Fig. 5. Advected heat flux through 300 and 750 km depth, respectively. (a) Case STD1. (b) STD2. (c) STD3. (d) BCLS1.

bottom (model BNOR1), straight penetration of the slab continues for the whole model run. With a closed, free-slip bottom boundary (BCLS1), episodes of penetration and of arresting the slab in the transition zone alternate (Fig. 5d) and give rise to a tortuous slab structure (Fig. 4e). With $U_{Trench} = 3$ cm/a no penetration was found irrespective of the bottom boundary condition (case BNOR3).

In the presence of trench retreat, straight penetration of a slab into the lower mantle at a constant dip angle requires flow from below the subducting plate to underneath the overriding plate. In the Earth, this will occur as part of the global three-dimensional circulation, for example around the edges of the slab. In the two-dimensional models, it can be achieved by flow through an artificial open bottom of the box (periodic side boundary conditions would be another way to allow for it). The higher the resistance against such flow, the larger is the tendency for the dip angle to become shallower and for the formation of flat slabs in the transition zone. Because some viscous resistance against flow 'around the slab' must exist in the Earth, the cases with a finite resistance at the bottom are perhaps the most realistic ones, although the best value of the R parameter is hard to estimate.

In model STD3-1, the trench moves at a rate of 3 cm/a until 40 Ma; thereafter it is slowed down to 1 cm/a. In response, the slab breaks through into the lower mantle at 50 Ma (Fig. 6b) at the location where new lithosphere descends (style FS, similar to Fig. 4c, but with a longer flat extension to the right),

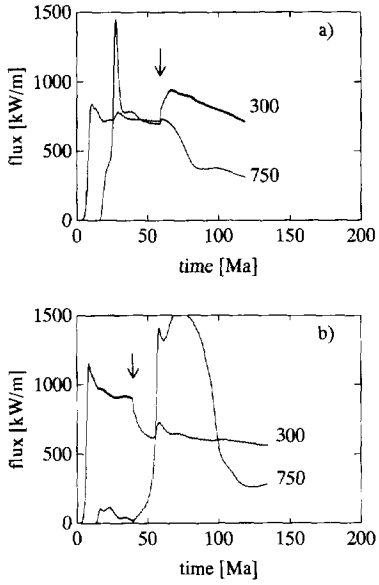

Fig. 6. Advected heat flux through 300 and 750 km depth, respectively. (a) Case STD1-3. (b) Case STD3-1. Arrows indicate the instant at which U_{Trench} changes.

and the flat slab segment is also dragged down. Eventually the slab flattens again in the transition zone, but continues to descend into the lower mantle at a reduced rate. In case STD1-3, trench motion is increased from 1 to 3 cm/a after 60 Ma. The slab, which up to this point descended straight into the lower mantle, starts to flatten immediately, and the slab flux into the lower mantle is reduced to about 40% of the subduction flux (Fig. 6a). In the model where the trench moved at 3 cm/a from the beginning, no significant penetration into the lower mantle was found. In the case STD1-3, the 'anchor' in the lower mantle, which was formed in the early stage of slow trench retreat, is important to ensure the ongoing penetration at the 'knee' of slab structure. This shows that, although the slab behaviour is primarily controlled by the instantaneous rate of trench migration, the past subduction history also has some influence.

3.2. Variation of parameters

3.2.1. Viscosity (Rayleigh number)

In a set of model runs, η_0 (Eq. (1)) was changed to 2×10^{20} Pa s or to 5×10^{19} Pa s, respectively, thus reducing or increasing the Rayleigh number by a factor of two (or changing the free sinking velocity of slabs by a factor two). With $U_{Trench} = 2$ cm/a, a lower viscosity leads to qualitatively similar behaviour as in the standard case (style FE) with slightly higher slab flow into the lower mantle (case LVIS2). When the viscosity is increased by a factor of two (HVIS2), a flat slab without penetration persisted for the entire model run (style F). Therefore, a higher free sinking velocity of the slab favours penetration into the lower mantle.

3.2.2. Reduced density contrast at 660 km

The olivine component makes up about two-thirds in the pyrolite model of the mantle [29], the remaining third being in the majorite–garnet phase in the transition zone. Majorite is also expected to transform to perovskite; however, the Clapeyron slope is highly uncertain and may be positive [30,31]. Here I assume $\gamma = 0$ for majorite, which reduces the dynamically active density contrast of the 660 km discontinuity from 9% to 6%. Qualitatively, the slab behaviour is comparable to that in the standard cases with slower trench velocity. With $U_{Trench} = 3$ cm/a (case LDC3) partial penetration is found, similar to case STD2 (shown in Fig. 4d), whereas for 4 cm/a of trench rollback (LDC4) a flat slab persists for the whole run.

3.2.3. Olivine–spinel boundary added

For the exothermic olivine–spinel transition a density contrast of 6%, a Clapeyron slope of +3 MPa/K, and a depth of 410 km at ambient temperature are assumed [32]. Slab penetration into the lower mantle is slightly favoured by the addition of the olivine–spinel boundary and U_{Trench} must be increased to 4 cm/a to prevent it entirely (OLS4). For 3 cm/a the slab flattens initially in the transition zone, but after 28 Ma it breaks through the 660 km boundary (OLS3, style FS). The additional negative buoyancy from the elevation of the olivine–spinel boundary causes the dip angle in the upper mantle to steepen, for example in case OLS4 to 65° from 50° in model STD4. The same effect is also observed when the viscosity is reduced (model LVIS3).

3.2.4. Viscosity step at 660 km

When the viscosity of the lower mantle is increased by a factor of five in a sharp additional rise at 660 km depth (broken line in Fig. 2), penetration of the slab occurs for $U_{Trench} = 1$ cm/a (VSTP1), but is already prevented for 2 cm/a (VSTP2) (Fig. 4f). Furthermore, in both cases the slab buckles. In model VSTP1, buckling starts as soon as the slab enters the lower mantle, in VSTP2 it begins after about 70 Ma (Fig. 7).

3.2.5. Different plate velocities

In two sets of models, the plate velocity was increased to 8 cm/a (UPL82–UPL84) or reduced to 3 cm/a (UPL31 and UPL32). The initial plate age at the trench was kept at 100 Ma. The critical trench velocity for the transition between penetration into the lower mantle and flattening of the slab was reduced to between 1 and 2 cm/a for the lower plate velocity and was not changed for $U_{Plate} = 8$ cm/a relative to the standard case. For a fixed trench velocity of 3 cm/a, U_{Plate} must be increased to 11 cm/a for penetration to occur (case UPL113). In case UPL83 the flattened slab buckles later. One of the fold loops is found to extend clearly below the

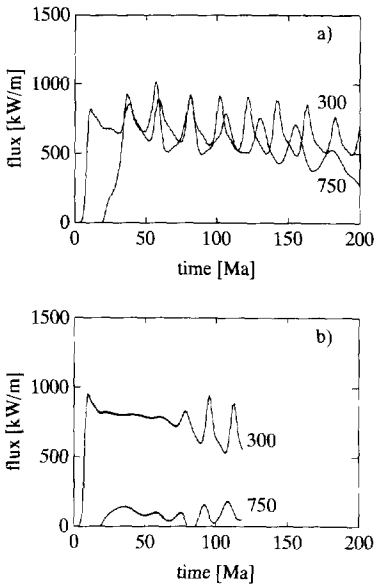

Fig. 7. Advected heat flux through 300 and 750 km depth, respectively. (a) Case VSTP1. (b) Case VSTP2. The oscillations are caused by slab folding.

phase boundary (Fig. 8) and it continues to sink, although only with about 0.9 cm/a in this stage.

3.2.6. Plates of different age

Van der Hilst and Seno [5] suggested that the age of the descending lithosphere also controls slab behaviour, with greater age favouring penetration. In two runs, the initial age, t_0, of the plate was reduced to 50 Ma and its initial length to 2500 km (cases AGE50.2 and AGE50.3). In another case t_0 was 150 Ma, the length of the plate 7500 km, and the box length 10,000 km (AGE150.3). No qualitative difference in the penetration style compared to the standard cases with the same trench velocities was found.

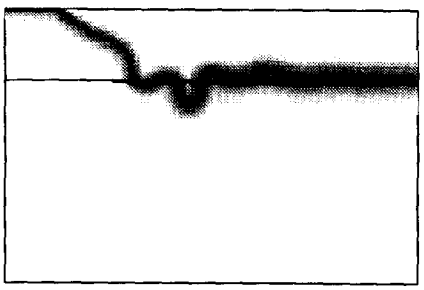

Fig. 8. Model UPL83, $U_{Plate} = 8$, $U_{Trench} = 3$ cm/a, after 79 Ma.

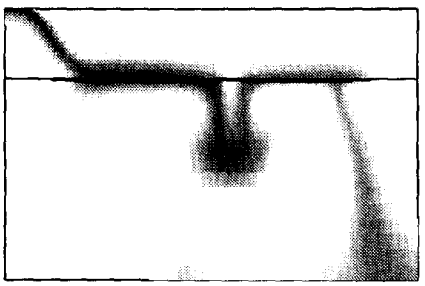

Fig. 9. Case AVIS1 after 267 Ma. The structure in the lower mantle on the right is the remainder of a previous diapir.

3.2.7. Slabs of ambient viscosity

In order to determine the influence of the high viscosity of the slab, in a set of models the parameter a in Eq. (1), which controls the degree of temperature dependence of viscosity, increases as a function of depth from its standard value above 300 km to infinity (no temperature dependence) below 400 km. At shallow depth the temperature dependence was kept so that the initial stage of subduction was the same as in the other cases. No immediate penetration of the cold downwelling was observed, even without trench migration (AVIS0); rather, the cold material spread above the phase boundary. For trench velocities below 3 cm/a (models AVIS0–AVIS2), this layer eventually becomes unstable and sinks in the form of a large diapir into the lower mantle (Fig. 9). The diapirs do not necessarily form below the subduction zone. For $U_{Trench} = 3$ cm/a (AVIS3) no significant penetration was observed during the time of the model run.

4. Discussion

For a stationary trench, the results confirm previous conclusions [16–18] that a high-viscosity slab penetrates more easily than a constant viscosity downwelling, although the long-term flux is rather similar in both cases. Trench migration tends to retard slab penetration into the lower mantle and facilitates the formation of flattened slabs above the 660 km discontinuity, as previous studies suggested [17,20–22,33]. However, most of these studies considered the 660 km discontinuity as a step in viscos-

ity and, in some cases, in intrinsic density, whereas in the present models the localised buoyancy of phase boundary distortion is the main obstacle to penetration into the lower mantle. An important difference is that once a segment of the slab descends below the phase boundary, its further sinking is not resisted by buoyancy forces. This gives rise to the style FE, which has not been described before, where a flattened slab bends down at its end and sinks into the lower mantle. The Tonga slab seems to deform in this way [4].

Buckling is observed in cases with a localised jump in viscosity at 660 km depth or with a high ratio of convergence velocity to free sinking velocity. Buckling would explain the broadening of slabs seen in many regional tomographic studies, although part of this might only be apparent because of a lack of resolution.

Unlike the 'avalanches' observed in many convection models, the change from a non-penetrative to a penetrative style is not accompanied by a drastic increase of flux into the lower mantle. In the present models, the slab flux into the lower mantle reaches peak values not much in excess of twice the subduction flux into the upper mantle. This is mostly a consequence of the high slab viscosity. To some extent, the imposed constant plate velocity in the model inhibits strong changes at depth. However, a large plate, such as the Pacific plate, is connected to several slabs that show a variety of deformation styles in the transition zone. The plate velocity must be controlled by the ensemble of slabs and is probably not strongly affected by events related to a single slab. For the same reason, two-dimensional models with a single slab, in which the plate velocity and rate of trench migration are not imposed but result from the model dynamics [19,33], may overestimate the feedback of deep processes on the plate kinematics. The present model concept, although simpler, allows the influence of plate kinematics on slab behaviour to be determined in a controlled way.

In the laboratory results of Guillou-Frottier et al. [22], piling-up of the subducted slab was much more prominent than in the present models; only for extreme rates of trench migration was a flat, undeformed slab deposited on the interface. The reason is probably that, in most of those models, the free sinking velocity of slabs in the lower layer was much smaller than the imposed subduction velocity. In the experiments of Griffiths et al. [21], where the difference in viscosity between the slab and the upper layer was only of order ten in most cases, penetration of an initially deposited slab occurred via a diapiric instability (style FD, illustrated in Fig. 9). Here, diapiric penetration is found only when the 'slab' has the same viscosity as its environment. In the Earth it may be relevant in cases where a slab is delayed in the transition zone long enough to heat up substantially.

Griffiths et al. [21] and Guillou et al. [22] attempted to explain the transition between the different observed regimes based on the ratio of the kinematically imposed velocities and the free sinking velocity of a slab. For this purpose, Griffiths et al. scaled the trench velocity with the sinking velocity in the upper layer, whereas Guillou et al. used the horizontal velocity of the slab at the point where it hits the interface, scaled with the sinking velocity in the lower layer. Because the behaviour of the slab in the transition zone is influenced by the dip angle, which depends on the sinking velocity in the upper layer, I use the free sinking velocity, U_{Sink}, of a detached slab extending from 200 to 600 km depth for scaling. U_{Sink} is determined by numerical experiment. In the standard cases $U_{Sink} = 11.8$ cm/a, whereas, in the cases with an additional five-fold viscosity increase at 660 km, U_{Sink} is only 4.9 cm/a because the slab already feels the high viscosity of the lower mantle. Fig. 10 shows the dependence of

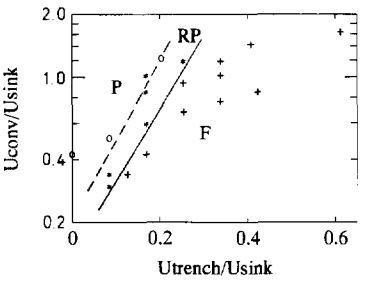

Fig. 10. Style of slab behaviour for all models with standard phase boundary parameters as function of the scaled trench migration velocity and the scaled convergence velocity. P and o = direct penetration; RP and * = retarded penetration; F and + = flat slab above the phase boundary.

the penetration regime on the scaled trench velocity and on the scaled velocity of convergence, $U_{Conv} = U_{Plate} + U_{Trench}$, for the cases with standard properties of the boundary. Everything else being equal, a high trench velocity prevents penetration whereas a high velocity of convergence relative to the free sinking velocity of the slab favours it.

What is the ultimate fate of a flat slab deposited above the 660 km discontinuity? In an otherwise stagnant mantle, it would slowly broaden by thermal diffusion while its peak temperature anomaly became less. The integrated negative thermal buoyancy in a vertical column would remain constant in this process. To stabilise the slab, its 'weight' must be compensated by an equal positive buoyancy force from phase boundary deflection. The peak temperature anomaly in the centre of the slab determines the maximum possible phase boundary deflection and, since it diminishes with time, at some point the slab must become unstable (a requirement is that the 660 km discontinuity is not globally covered with dead slabs). A quantitative consideration (Appendix A arrives at a time scale of a few hundred million years for this to occur. This was confirmed by a numerical experiment, where a 100 Ma old slab, lying horizontally on the phase boundary, was taken as the initial state in a model without surface motion. Breakthrough into the lower mantle started after 290 Ma. The general circulation in the mantle would tend to destabilise the slab earlier, whereas gravitational spreading of the slab would delay it (Appendix A. If a flat slab already has an 'anchor' in the lower mantle, this will pull the slab down before the destabilisation mechanism described before could act.

The critical rate of trench migration, above which flattening of the slab occurs, could be influenced by several unmodelled effects. A strongly positive Clapeyron slope for the transition of majorite to perovskite would push the limit to higher trench velocities. The retarded transition of Al-rich garnet to perovskite in the former oceanic crust, which is, according to Ringwood and Irifune [29], not completed above 750 km depth, has a similar effect as adding -0.7 MPa/K to the Clapeyron slope [17]. A rather stronger effect favouring the formation of flat slabs could be expected if the stability of garnet in the former crust extends to much greater depth, which has been recently proposed [34], but is disputed [35]. The exothermic olivine spinel transition should slightly favour penetration, but its dynamic influence depends on the degree by which the transition is kinematically retarded in the coldest part of the slab [36,37]. For old and fast subducting slabs it may oppose penetration. A strong kinetic barrier against the transformation from spinel to perovskite could be even more important, but so far little is known about the importance of kinetic effects for this transition. A much stronger increase in viscosity with depth in the lower mantle than has been assumed here, which is suggested by the steep melting point gradient found by Zerr and Boehler [38], could also favour slab flattening.

The parameters in the model calculations span a range reasonably close to Earth values and therefore the results can be applied directly. They suggest that flattening of the slab is to be expected when the trench velocity exceeds 2–4 cm/a. For the Earth, a typical rate of trench migration is on the order of 1–3 cm/a [39]. Higher velocities are possible when back-arc spreading occurs, but then the estimates become more uncertain. Based on tectonic reconstructions [4,5] and geodetic measurements [40], high rates of trench rollback have been inferred for the Tonga and Izu–Bonin slabs which flatten in the transition zone. Overall, the predicted critical trench velocity in the range of 2–4 cm/a seems compatible with the available observations.

The global study of SS precursors by Shearer and Masters [6] suggests that there is considerable long-wavelength topography on the 660 km discontinuity. Subduction zones are associated with depressions of about 15 km amplitude on a regional scale. Although the peak depression in the model cases with straight slab penetration is about 50 km, it is necessarily localised, and the mean depression taken over an averaging length of 2200 km (the resolving length in Shearer and Masters' inversion) is only 3.8 km. For the flat slab of Fig. 4b the mean depression averaged on the same length scale is 26 km. Solheim and Peltier [15] found that the observed variance of the 660 km discontinuity is compatible with an episodically layered convection model. From comparing my model results with the observed 660 km topography near subduction zones, I conclude more specifically that flat-lying slabs in the transition zone must be fairly common.

5. Conclusions

Semi-kinematic convection models, which try to capture some essential characteristics of the subduction process, indicate that moderate rates of trench rollback can lead to a deflection of slabs by the endothermic phase change at 660 km depth. This agrees with the seismological evidence for the coexistence of flat subhorizontal slabs above the 660 km discontinuity and for slabs extending straight into the lower mantle in various subduction zones. The age of the slab has no strong influence on penetration. Flattened slabs are only temporarily arrested in the transition zone. They are either slowly pulled into the lower mantle by an attached slab segment that has already descended below 660 km, or they are eventually destabilised and sink after warming and broadening by thermal diffusion. While penetration of slabs into the lower mantle is episodic in time, it is probably not characterised by vigorous 'avalanche' events.

Acknowledgements

Comments by John Castle, Moritz Heimpel, Michael Weber, and Chuck Wicks improved the manuscript. Supported by the Deutsche Forschungsgemeinschaft through grant Ch77/8. *[FA]*

Appendix A

A stagnant flat-lying slab whose weight is compensated by the deflection of an endothermic phase boundary is considered. Heat transport is assumed to be only by conduction in the vertical direction. For simplicity, the initial profile of the temperature anomaly $\Delta T(z, t = 0)$ is taken to be Gaussian, because it then remains self-similar. The width of the initial profile is controlled by a nominal age, t_o, and the peak temperature anomaly is $T(z = 0,t = 0) = T_1$. The temperature anomaly as a function of time $t > 0$ is:

$$\Delta T = T_1 \left(\frac{t_o}{t + t_o} \right)^{1/2} \exp \left(\frac{-z^2}{4\kappa(t + t_o)} \right) \qquad (A1)$$

The integrated thermal anomaly is constant with time and equal to the anomaly in an error-function distribution of the same nominal age, t_o, and amplitude, T_o, when $T_1 = T_o/\pi$. The total thermal buoyancy is:

$$B_T = 2T_1 \rho \alpha g (\pi \kappa t_o)^{1/2} \qquad (A2)$$

The maximum possible deflection, Δz_{max}, of the phase boundary is given by $\rho g \Delta z_{max} = \gamma \Delta T(z = 0,t)$, and the associated buoyancy force is:

$$B_{P,max} = \Delta \rho g \Delta z_{max} = \gamma \Delta_\rho / \rho T_1 (t_o / [t + t_o])^{1/2} \qquad (A3)$$

The slab will be stable as long as $B_{P,max} > B_T$, which leads to the condition:

$$t_o + t < \frac{1}{4\pi\kappa} \left(\frac{\gamma \Delta \rho}{\rho^2 \alpha g} \right)^2 \qquad (A4)$$

For $\alpha = 2 \times 10^{-5}$ K^{-1} and other parameters as in Table 1, the condition results in $t + t_o < 250$ Ma. This agrees on an order of magnitude scale with the result of the numerical experiment for a flat-lying slab, in which instability occurred after $t = 290$ Ma. In this experiment a slow gravitational spreading of the slab was observed, which reduces B_T with time. It also leads to a faster reduction of the peak thermal anomaly. When a pure shear mode of horizontal extension is assumed, the Gaussian temperature profile still remains self-similar, and a similar analysis to that above can be done (not presented here). It shows that the first effect (reduction of B_T) is dominant, which explains the delayed onset of instability.

References

[1] R. Van der Hilst, E.R. Engdahl, W. Spakman and G. Nolet, Tomographic imaging of subducted lithosphere below Northwest Pacific island arcs, Nature 353, 37–43, 1991.

[2] Y. Fukao, M. Obayashi, H. Inoue and M. Nenbai, Subducting slabs stagnant in the transition zone, J. Geophys. Res. 97, 4809–4822, 1992.

[3] S.P. Grand, Mantle shear structure beneath the Americas and the surrounding oceans, J. Geophys. Res. 99, 11591–11621, 1994.

[4] R. Van der Hilst, Complex morphology of subducted lithosphere in the mantle beneath the Tonga trench, Nature 374, 154–157, 1995.

[5] R. Van der Hilst and T. Seno, Effects of relative plate motion on the deep structure and penetration depth below the Izu–Bonin and Mariana island arcs, Earth Planet. Sci Lett. 120, 395–407, 1994.

[6] P.M. Shearer and T.G. Masters, Global mapping of topography on the 660-km discontinuity, Nature 355, 791–796, 1992.

[7] C.W. Wicks and M.A. Richards, A detailed map of the 660-kilometer discontinuity beneath the Izu–Bonin subduction zone, Science 261, 1424–1427, 1993.

[8] E. Ito and E. Takahashi, Postspinel transformations in the system Mg_2SiO_4–Fe_2SiO_4 and some geophysical implications, J. Geophys. Res. 94, 10637–10646, 1989.

[9] L. Stixrude, R.J. Hemley, Y. Fei and H.-K. Mao, Thermoelasticity of silicate perovskite and magnesiowüstite and stratification of the Earth's mantle, Science 257, 1099–1101, 1992.

[10] U.R. Christensen and D.A. Yuen, The interaction of a subducting lithospheric slab with a chemical or phase boundary, J. Geophys. Res. 89, 4389–4402, 1984.

[11] C.R. Bina and G. Helffrich, Phase transition Clapeyron slopes and transition zone seismic discontinuity topography, J. Geophys. Res. 99, 15853–15860, 1994.

[12] U.R. Christensen and D.A. Yuen, Layered convection induced by phase transitions, J. Geophys. Res. 90, 10291–10300, 1985.

[13] P. Machetel and P. Weber, Intermittent layered convection in a model with an endothermic phase change at 670 km, Nature 350, 55–57, 1991.

[14] P.J. Tackley, D.J. Stevenson, G.A. Glatzmaier and G. Schubert, Effects of an endothermic phase transition at 670 km depth in a spherical model of convection in the Earth's mantle, Nature 361, 699–704, 1993.

[15] L.P. Solheim and W.R. Peltier, 660 km phase boundary deflections and episodically layered isochemical convection, J. Geophys. Res. 99, 15861–15875, 1994.

[16] S. Zhong and M. Gurnis, Role of plates and temperature-dependent viscosity in phase change dynamics, J. Geophys. Res. 99, 15903–15917, 1994.

[17] G.F. Davies, Penetration of plates and plumes through the mantle transition zone, Earth Planet. Sci. Lett. 133, 507–516, 1995.

[18] S.D. King and J. Ita, Effect of slab rheology on mass transport across a phase transition boundary, J. Geophys. Res. 100, 20211–20222, 1995.

[19] S. Zhong and M. Gurnis, Mantle convection with plates and mobile, faulted plate margins, Science 267, 838–843, 1995.

[20] C. Kincaid and P. Olson, An experimental study of subduction and slab migration, J. Geophys. Res. 92, 13832–13840, 1987.

[21] R.W. Griffiths, R.I. Hackney and R. Van der Hilst, A laboratory investigation of effects of trench migration on the descent of subducted slabs, Earth Planet. Sci. Lett. 133, 1–18, 1995.

[22] L. Guillou-Frottier, J. Buttles and P. Olson, Laboratory experiments on the structure of subducted lithosphere, Earth Planet. Sci. Lett. 133, 19–34, 1995.

[23] B.H. Hager and M.A. Richards, Long-wavelength variations in Earth's geoid: physical models and dynamical implications, Philos. Trans. R. Soc. London A 328, 309–327, 1989.

[24] A.M. Forte and R. Peltier, Viscous flow models and global geophysical observables 1. Forward problems, J. Geophys. Res. 96, 20131–20159, 1991.

[25] U. Christensen, Convection with pressure- and temperature-dependent non-Newtonian rheology, Geophys. J. R. Astron. Soc. 77, 343–384, 1984.

[26] A. Chopelas and R. Boehler, Thermal expansivity of the lower mantle, Geophys. Res. Lett. 19, 1983–1986, 1992.

[27] J. Ita and S. King, The sensitivity of convection with an endothermic phase change to the form of governing equations, initial conditions, boundary conditions, and equation of state, J. Geophys. Res. 99, 15919–15938, 1994.

[28] U.R. Christensen, An Eulerian technique for thermomechanical modeling of lithospheric extension, J. Geophys. Res. 97, 2015–2036, 1992.

[29] A.E. Ringwood and T. Irifune, Nature of the 650-km seismic discontinuity: implications for mantle dynamics and differentiation, Nature 331, 131–136, 1988.

[30] T. Gasparik, Phase relations in the transition zone, J. Geophys. Res. 95, 15751–15769, 1990.

[31] H. Yusa, M. Akaogi and E. Ito, Calorimetric study of $MgSiO_3$ garnet and pyroxene: heat capacities, transition enthalpies, and equilibrium phase relations in $MgSiO_3$ at high pressures and temperatures, J. Geophys. Res. 98, 6453–6460, 1993.

[32] T. Katsura and E. Ito, The systems Mg_2SiO_4–Fe_2SiO_4 at high pressures and temperatures: precise determination of stabilities of olivine, modified spinel, and spinel, J. Geophys. Res. 94, 15663–15670, 1989.

[33] M. Gurnis and B.H. Hager, Controls on the structure of subducted slabs, Nature 335, 317–321, 1988.

[34] B. O'Neill and R. Jeanloz, $MgSiO_3$–$FeSiO_3$–Al_2O_3 in the Earth's lower mantle: perovskite and garnet at 1200 km depth, J. Geophys. Res. 99, 19901–19915, 1994.

[35] S.E. Kesson, J.D. Fitzgerald, J.M.G. Shelley and R.L. Withers, Phase relations, structure and crystal chemistry of some aluminous perovskites, Earth Planet. Sci. Lett. 134, 187–201, 1995.

[36] H.W. Green and H. Houston, The mechanics of deep earthquakes, Annu. Rev. Earth Planet. Sci. 23, 169–213, 1995.

[37] R. Daessler and D.A. Yuen, The effects of phase transition kinetics on subducting slabs, Geophys. Res. Lett. 20, 2603–2606, 1993.

[38] A. Zerr and R. Boehler, Melting of $(Mg,Fe)SiO_3$–perovskite to 625 kilobars: indication of a high melting temperature in the lower mantle, Science 262, 553–555, 1993.

[39] Z. Garfunkel, C.A. Anderson and G. Schubert, Mantle circulation and the lateral migration of subducted slabs, J. Geophys. Res. 91, 7205–7223, 1986.

[40] M. Bevis, F.W. Taylor, B.E. Schutz, J. Recy, B.L. Isacks, S. Helu, R. Singh, E. Kendrick, J. Stowell, B. Taylor and S. Calmant, Geodetic observation of very rapid convergence and back-arc extension at the Tonga arc, Nature 374, 249–251, 1995.